The Astrophysical Journal, 696:1600–1611, 2009 May 10 doi:10.1088/0004-637X/696/2/1600

FORMATION, SURVIVAL, AND DETECTABILITY OF PLANETS BEYOND 100 AU

Dimitri Veras[1], Justin R. Crepp[1,2], and Eric B. Ford[1]
[1] Astronomy Department, University of Florida, 211 Bryant Space Sciences Center, Gainesville, FL 32111, USA; veras@astro.ufl.edu
[2] California Institute of Technology, Department of Astronomy/Optical Observatories, 1216 E. California Boulevard, Pasadena, CA 91126, USA
Received 2008 December 16; accepted 2009 February 13; published 2009 April 27

ABSTRACT

Direct imaging searches have begun to detect planetary and brown dwarf companions and to place constraints on the presence of giant planets at large separations from their host star. This work helps to motivate such planet searches by predicting a population of young giant planets that could be detectable by direct imaging campaigns. Both the classical core accretion and the gravitational instability model for planet formation are hard pressed to form long-period planets in situ. Here, we show that dynamical instabilities among planetary systems that originally formed multiple giant planets much closer to the host star could produce a population of giant planets at large ($\approx 10^2$–10^5 AU) separations. We estimate the limits within which these planets may survive, quantify the efficiency of gravitational scattering into both stable and unstable wide orbits, and demonstrate that population analyses must take into account the age of the system. We predict that planet scattering creates detectable giant planets on wide orbits that decreases in number on timescales of $\sim$ 10 Myr. We demonstrate that several members of such populations should be detectable with current technology, quantify the prospects for future instruments, and suggest how they could place interesting constraints on planet formation models.

Key words: celestial mechanics – methods: *N*-body simulations – open clusters and associations: general – planetary systems: formation – stars: imaging – techniques: high angular resolution

Online-only material: color figures

1. INTRODUCTION

Recently, several high-contrast imaging campaigns have begun to search for young giant planets orbiting relatively nearby stars at large orbital separations. In addition to compelling detections of likely planetary systems (e.g., Kalas et al. 2008; Marois et al. 2008), surveys of young stars have placed significant constraints on the presence of any giant planets at large separations (e.g., McCarthy & Zuckerman 2004; Kasper et al. 2007; Lafrenière et al. 2007; Nielsen et al. 2007). In the near future, even more powerful searches have the potential to detect even lower mass planets in wide orbits around nearby stars. These surveys could reveal new populations of extrasolar planets, since planets with long ($\gtrsim 10^2$ yr) periods are difficult to detect by most planet search techniques such as radial velocities, astrometry, transit photometry, and even microlensing.

The frequency and orbital properties of long-period planets could provide interesting constraints for planet formation models. The core accretion model struggles even to explain the in situ accretion of Uranus and Neptune, given the need to form a rocky core while there is still significant gas in the circumsolar nebula (Pollack et al. 1996; Goldreich et al. 2004). This timescale problem has led to several models in which Uranus and Neptune form closer to the Sun and migrate outward to their present locations (e.g., Thommes et al. 1999, 2002; Gomes et al. 2005; Morbidelli et al. 2005; Tsiganis et al. 2005; Ford & Chaing 2007). Given these difficulties at 40 AU, the standard core accretion model is unable to form giant planets at much larger separations such as $\sim$ 1000 or even $\sim$ 100 AU. Alternatively, the gravitational instability model may become more plausible at large separations (Rafikov 2005; Stamatellos & Whitworth 2009). Hence, some recent ground-based direct detection campaigns have framed their searches as a way to search for planets that could *not* be formed by core accretion, and thus provide support for some planets having formed via gravitational instability. However, recent research has also cast doubt on the viability of the gravitational instability model (Mejía et al. 2005; Cai et al. 2005; Boss 2006; Rafikov 2007). Therefore, one might worry that a non-detection by direct imaging planet searches (e.g., Kasper et al. 2007; Lafrenière et al. 2007; Nielsen et al. 2007) would fail to provide new constraints on planet formation models. In this paper, we show that this is not the case. In either the core accretion or gravitational instability model, the formation of multiple giant planets at moderate separations ($\sim$1–10 AU) naturally leads to dynamical instabilities that result in one or more planets being scattered into very wide ($\approx 10^2$–10^5 AU) orbits. Thus, direct imaging searches (such as The Gemini Planet Imager (GPI); Macintosh et al. 2006a) and microlensing planet searches have the potential to place significant constraints on the frequency of dynamically active planetary systems that form multiple giant planets.

Extrasolar giant planets have a broad range of eccentricities. Although several proposed mechanisms may explain the eccentricities of some planets, the high frequency of eccentric orbits among giant planets suggests that dynamical instabilities resulting in planet–planet scattering play an important role in sculpting many planetary systems. Although many variations of the planet–planet scattering model have been explored (e.g., Rasio & Ford 1996; Weidenschilling & Marzari 1996; Levison et al. 1998; Ford et al. 2001; Marzari & Weidenschilling 2002; Adams & Laughlin 2003; Veras & Armitage 2004, 2006; Moorhead & Adams 2005; Chatterjee et al. 2008; Ford & Rasio 2008; Juric & Tremaine 2008), these studies focused on the final properties of the bound planets and paid little attention to the orbital evolution of planets that will eventually be ejected from the system. de la Fuente Marcos & de la Fuente Marcos (2001) demonstrate how Kuiper Belt Objects can be scattered outward to hundreds or thousands of AU, and recently, a dynamical in-

stability has been suggested as a possible formation mechanism for the substellar companion to GQ Lup (Debes & Sigurdsson 2006) in a wide ($\approx$ 100 AU) orbit. However, previous dynamical studies have yet to quantify the probability for scattered planets to be detected via direct imaging. We investigate the orbital properties and lifetime of planets scattered into wide orbits and assess the prospects for their detection via high-contrast imaging. Our study complements that of Scharf & Menou (2009), as we consider additional effects, including galactic tides, scattering of terrestrial-mass planets, and observational estimates of the contrast for long-period giant planets.

Given the history of extrasolar planets repeatedly being discovered in unexpected locations, it is worth searching for planets anywhere that they could survive. Therefore, we begin by exploring the physical limits that can be placed on very long period planets and find that planets could survive with orbital separations of up to $\sim 10^5$ AU in Section 2. Such estimates can be compared with the separations at which planets are observed in order to determine whether there are additional processes shaping this distribution. In Section 3, we describe a model where multiple giant planets form at traditional orbital separations ($\sim$ 3–30 AU). As the disk dissipates, the planets will perturb each other, eventually resulting in eccentricity growth, close encounters, and some planets being ejected from the planetary system (Chatterjee et al. 2008). Before the planets are ejected, they will spend considerable time at very large orbital separations from the host star. Thus, planet scattering should result in a significant number of giant planets being scattered onto very wide orbits, where they could be detected by recent or future direct imaging planet searches. By quantifying the efficiency of scattering onto such orbits, we estimate how large a sample needs to be surveyed in order to detect such planets. We additionally explore the timescale on which detectable wide-orbit planets remain; we predict that the population of unstable planets "passing through" a wide-orbit phase is larger than the population of planets on stable wide orbits. The existence of this population does not require that either the standard core accretion or the gravitational instability mechanism be able to form giant planets at large separations, where direct imaging campaigns are most sensitive. Observations of these planets at different ages can impart information about the chaotic stage of planet formation (e.g., how many giant planets are typically formed before planet scattering widdles down the number of surviving planets to 2 or 3). Finally, we consider the prospects for a direct imaging campaign to detect such planets and their implications in Section 4. System age, contrast, and separation limits all affect population analyses from such campaigns.

2. SURVIVAL AND DESTRUCTION OF LONG-PERIOD PLANETS

We begin by asking what processes would limit the survival of very long period giant planets orbiting main-sequence stars. Most previous studies investigating the effects of passing stars have focused on planets at separations $\leqslant$ 40 AU (e.g., Laughlin & Adams 1998; Ford et al. 2000a; Adams et al. 2006). If giant planets have much larger orbits, then the effects of stellar encounters could be dramatically increased. In the limit that planets are much less massive than stars, they can be treated as test particles, allowing us to apply many arguments previously applied to the survival of long-period comets.

2.1. Field Stars

First, we consider the constraints on long-period planets around field stars in the galactic disk, closely following the treatment of Tremaine (1993).

2.1.1. Galactic Tide

Planets in sufficiently wide orbits will be influenced by gravitational perturbations from the galactic tides. Like comets, a planet will typically become unbound if the star–planet separation exceeds the tidal radius, estimated by

$$a_t \simeq 1.7 \times 10^5 \text{ AU} \left(\frac{M_\star}{M_\odot}\right)^{1/3} \left(\frac{\rho}{0.1\ M_\odot\ \text{pc}^{-3}}\right)^{-1/3}, \quad (1)$$

where $M_\star$ is the mass of the host star and ρ is the local galactic mass density (Tremaine 1993). Once a planet is scattered beyond a_t, it will likely become unbound on an orbital timescale.

2.1.2. Passing Stars

Encounters with passing stars and giant molecular clouds can eject a planet, either by a single encounter or by repeatedly perturbing the planet's orbit. Weinberg et al. (1987) calculate that half-life of a long-period planet in the solar neighborhood due to the cumulative effect of many encounters with passing stars to be

$$\tau_{\text{ps}} \simeq 10 \text{ Gyr} \left(\frac{M_\star}{M_\odot}\right) \left(\frac{10^4 \text{ AU}}{a}\right) \left(\frac{0.15\ M_\odot\ \text{pc}^{-3}}{\rho}\right), \quad (2)$$

where a is the planet's semimajor axis. Assuming that the planet either formed in situ or migrated to its current location on a timescale much less than the system age, we can equate the timescale for a planet to become unbound to the age of the star, resulting in an estimate of the maximum distance at which a planet is likely to survive,

$$a_{\text{ps}} \simeq 10^5 \text{ AU} \left(\frac{\text{Gyr}}{t_\star}\right) \left(\frac{M_\star}{M_\odot}\right) \left(\frac{0.15\ M_\odot\ \text{pc}^{-3}}{\rho}\right), \quad (3)$$

where $t_\star$ is the age of the star, and provided that $a_{\text{ps}} \ll a_t$. Thus, the limiting semimajor axis for young disk stars will be set by the tidal limit, while the limiting semimajor axis for old field stars will be set by the cumulative effect of many stellar encounters.

2.2. Stars in Clusters

Most disk stars formed in small clusters (Throop et al. 2001). Because the rate of stellar encounters depends strongly on the local stellar density, the effects of stellar encounters are likely dominated by interactions while the star is young and still in a dense young stellar cluster. If planets form or migrate to long-period orbits while the host star is still in a dense region of the cluster, then encounters with cluster members could place more stringent constraints than those discussed in Section 2.1. The importance of stellar encounters is linked to the dynamical evolution of the cluster in which the star formed. Following Adams et al. (2006), we separate the dynamical evolution of the cluster from the dynamics of close encounters.

2.2.1. Cross Sections for Impulsive Encounter with Single Stars

First, we consider the ejection of planets in a single encounter. The timescale for a stellar encounter to eject a planet from its host star can be estimated by $\tau^{-1} \sim \langle n_\star \sigma v_\infty \rangle$, where $n_\star$ is the local density of stars, v_∞ is the velocity at infinity of the passing star, σ is the relevant cross section, and $\langle\rangle$ indicates a time average. For very long period planets, encounters with single stars are impulsive when

$$a > a_{\rm imp} \simeq 890 \text{ AU} \left(\frac{M_1 + m}{M_\odot} \right) \left(\frac{1 \text{ km s}^{-1}}{v_\infty} \right)^2, \quad (4)$$

where a is the semimajor axis and M_1 is the mass of the host star. In this regime, the cross section for ionizing the planet from the host star is

$$\sigma_{\rm ion} \simeq \frac{40\pi a G}{3 v_\infty^2} \frac{M_2^2}{M_1 + m} \simeq (193 \text{ AU})^2 \left(\frac{a}{\text{AU}} \right) \left(\frac{\text{km s}^{-1}}{v_\infty^2} \right)^2 \frac{M_2^2}{M_1}, \quad (5)$$

where M_2 is the mass of the passing star and G is the gravitational constant (Hut 1983; Equation (13) of Fregeau et al. 2006).

In addition to planets being ejected, some planets will be exchanged into orbit around the passing star. For the sake of comparing to the cross section for ionization, we consider equal-mass stars of mass $M = M_1 = M_2$, in which case

$$\sigma_{\rm ex_s(nonres)} \simeq \frac{20\pi}{3 a v_\infty^6} G^3 M^2 (M + m) \quad (6)$$

(Hut 1983;Equation (14) of Fregeau et al. 2006). For strongly impulsive encounters, the cross section for exchange is much less than the cross section for ionization, so exchanges are relatively insignificant.

2.2.2. Cross Section for Intermediate Encounter with Single Stars

For planets at somewhat shorter orbital periods ($a \leqslant 1000$ AU), the scattering behavior enters an alternative regime, where the cross sections for ionization and exchange are comparable. Numerical simulations for a circular planet encountering a single star find that

$$\sigma_{\rm ion} \simeq 1.2\pi a G M_t / v_\infty^2 \quad (7)$$

and

$$\sigma_{\rm ex_s(nonres)} \simeq 0.6\pi a G M_t / v_\infty^2 \quad (8)$$

were $M_t = M_1 + M_2 + m$ is the total mass (Equation (15) and Figure 3 of Fregeau et al. 2006). In this regime, when the planet is exchanged to the passing star, the binding energy of the planet before and after the star will be comparable (with a typical change of $\simeq$ 20%). Therefore, exchanges between stars of similar mass result in a planet orbit comparable to before the encounter. Among a coeval cluster of stars, such an exchange is unlikely to be recognizable, except in unusual circumstances (e.g., PSR 1620+26; Ford et al. 2000b).

2.2.3. Rate of Close Encounters for Stars in Clusters

Simulations of star clusters can be used to calculate the rate of stellar flybys. Table 3 from Adams et al. (2006) provides empirical fits to the results of their simulations, with the form

$$\Gamma = \Gamma_o \left(\frac{b}{1000 \text{ AU}} \right)^\gamma, \quad (9)$$

where b is the closest approach distance, and Γ_o and γ are the fit parameters (see Table 3 of Adams et al. 2006). For a typical cluster of 100–1000 stars, they find that a typical star undergoes $N(< 100 \text{ AU}) \sim 0.2$–2 or interactions with closest approach distance less than 100 AU over the course of a 10 Myr simulation. Similarly, they find $N(< 1000 \text{ AU}) \sim 1$–14 encounters coming within 1000 AU over the course of a 10 Myr simulation.

2.2.4. Ionization Rate by Single Encounters with Single Stars

We find the semimajor axis beyond which a planet will typically be ejected by a single encounter with a passing star by setting $b = \sqrt{\sigma_{\rm ion}/\pi}$. Thus, a typical planet will be ejected if the encounter is impulsive (i.e., $a > a_{\rm imp}$) and the planet's orbit exceeds

$$a_{\rm ps,imp} \simeq 85 \text{ AU} \left(\frac{(M_1 + m)\, M_\odot}{M_2^2} \right) \left(\frac{v_\infty}{\text{km s}^{-1}} \right)^2 \left(\frac{\text{Myr}}{\Gamma_o t} \right)^{2/\gamma}, \quad (10)$$

where t is the time available for stellar encounters. Similarly, a typical planet will be ionized if the encounters are in the intermediate regime identified by Fregeau et al. (2006) and

$$a_{\rm ps,int} \simeq 944 \text{ AU} \left(\frac{M_\odot}{M_t} \right) \left(\frac{v_\infty}{\text{km s}^{-1}} \right)^2 \left(\frac{\text{Myr}}{\Gamma_o t} \right)^{2/\gamma}. \quad (11)$$

For planets that form concurrently with the star and in situ, the final factor of Equations (10) and (11) ranges from $\simeq$ 0.5 to 6.9 for the 10 Myr simulations of small clusters with 100–1000 stars (Adams et al. 2006). Therefore, planets that form (or migrate) beyond $a_{\rm imp}$ during the earliest stages of the cluster would be ejected by a single impulsive stellar encounter. For some choices of cluster parameters (i.e., the "cold-start" simulations of Adams et al. 2006), planets inward of $a_{\rm imp}$ but beyond $a_{\rm ps,int}$ could be ionized by passing stars before the cluster dissolves.

The previous estimates assume that the planet forms in situ at the same time as the star. As we discussed in Section 1, some theoretical models predict that planets might form close to a star and then be scattered outward much later. For the same simulations, but considering planets that are placed at large separation 5 Myr into the cluster simulations, the final factor of Equations (10) and (11) ranges from $\simeq$ 4.6 to 190 (considering the subsequent 5 Myr evolution of the clusters; Adams et al. 2006). Therefore, planets that migrate to large separations after the cluster loses its gas (at 5 Myr in simulations of Adams et al. 2006) could avoid being disrupted by stellar encounters at separations of up to $\sim \max(a_{\rm imp}, a_{\rm ps,imp}) \sim 10^3$–$3 \times 10^4$ AU.

Most stars in a cluster are actually members of binary (or higher order multiple) star systems. For the wide planetary orbits of interest, encounters with close binaries proceed similarly to encounters with single stars. The primary difference is that encounters which previously resulted in the planet exchanging into orbit around the passing star now result in forming a triple system including the circumbinary planet. Encounters with binary stars that have larger orbital periods are more likely to result in ionization, as even exchange interactions often result in unstable triple systems that subsequently eject the lowest mass planet. Numerical simulations including a plausible distribution of binary mass ratios and periods verify that the cross section for ionization by binary systems is roughly comparable to the sum of the cross sections for ionization by the individual stars.

2.3. Summary of Survival of Long-Period Planets

In summary, interactions prior to the dissociation of the cluster can dominate the ionization of planets that form or migrate to large distances before the parent cluster dissociates. For planets that appear at large separations near the birth of the cluster, survival for the life of the cluster can require $a \leqslant 500$–6000 AU, depending on the cluster properties. However, if planets are able to form or migrate to very large separations more than a few million years after the formation of the cluster, then they could survive at much larger distances. A delay of 10 Myr is more than sufficient to allow planets to survive with semimajor axes approaching the tidal limit (or a_{ps} for old star).

In order to identify the most significant processes affecting planets in wide orbits, we compare several relevant timescales. The planet formation timescale is a key difference between the two leading models for planet formation: core accretion and gravitational instability (see Armitage 2007, for a recent summary). In the classical core accretion model, accretion of gas onto a giant planets at Jovian-like distances ($\sim$ 5 AU) lasts at least 8 Myr (Pollack et al. 1996). However, Haisch et al. (2001) estimates that the lifetimes of protostellar disks last at most $\approx$ 3 Myr, and this timescale imposes a maximum value on the core accretion timescale. This has inspired theoretical research to explore whether core accretion may be able to act more rapidly. Indeed, variations on the core accretion model are able to form planets more rapidly. For example, Hubickyj et al. (2005) find that the Jupiter could have formed in 2.2 Myr, and Dodson-Robinson et al. (2008) present two new models where Saturn forms at $\sim$ 12 AU in just under 3.5 Myr. Chambers (2006) envisages accretion times under 1 Myr. While further research is in order, it is unlikely that the core accretion timescale lies outside of 0.1–10 Myr. In the gravitational instability model, giant planets acquire their mass on much shorter timescales which are unlikely to surpass 10^4 yr (Durisen et al. 2007, and references therein).

After multiple planets have formed in a protoplanetary disk, they can begin to interact with each other. Initially, the gas disk can suppress eccentricity excitation, but once the gas dissipates, the system can rapidly become orbit crossing. Alternatively, for systems containing planets that are more widely spaced, the planets can remain on low-eccentricity orbits for over a billion years before chaotic evolution leads to orbit crossing. In either case, once orbits cross, close encounters and eccentric orbits soon follow (Chatterjee et al. 2008). Before a planet is to be scattered onto a very wide orbit or ejected from the system, it will undergo a series of many close encounters. The timescale depends on the planet masses and the orbital period of the more massive planet (that typically remains bound). For scattering by Jupiter, the median value of this timescale is $\sim$ 10^4 yr, with a range that spans several magnitudes (see Section 3.2).

The process which limits the orbital separation of long-period planets will vary from system to system, depending on the host star environment and the time until the planet is scattered onto a wide orbit. Most stars are believed to form in star clusters, groups, or associations that dissociate on timescales of a few Myr. Simulations of star clusters show that most of the close encounters occur during the first few million years. If planets form in situ in wide orbits (e.g., by gravitational instability) or if they migrate or are scattered into wide orbits very rapidly, then planets beyond $\sim$700–4000 AU could have been disrupted by passing stars before the host cluster dissociates (Adams et al. 2006). The width of the main sequence in open clusters suggests that stars in a larger cluster form within $\sim$ 5 Myr of each other (Bonatto & Bica 2009). Thus, it may be possible for planets formed via gravitational instability to survive at larger separations, if the planet orbits a star that formed a few Myr after the cluster's massive stars have started to remove the cluster's gas. For such planets and planets that are scattered into wide orbits shortly after the cluster dissociates, the tidal field of the molecular cloud can disrupt planets with separations exceeding $\sim$ 10^4–10^5 AU. For planets that are scattered into wide orbits well after the cluster has dissociated and the star has drifted away from the host molecular cloud, perturbations from passing stars and galactic tides can remove wide-period planets on timescales of $\sim$ Gyr (Equation (2); Higuchi et al. 2007).

3. FORMATION OF LONG-PERIOD PLANETS VIA PLANET–PLANET SCATTERING

When considering the survival of long-period planets in Section 2.1, we applied arguments previously developed for the survival of Oort cloud comets. However, the mechanisms responsible for creating the Oort cloud are unlikely to produce a large population of long-period planets. Populating the Oort cloud is inefficient, as only $\sim$2% of the parent population scattered by Jupiter and Saturn end up in bound orbits with very long periods, rather than being ejected from the system or colliding with a planet (Duncan et al. 1987; Dones et al. 2004; Higuchi et al. 2006; Brasser et al. 2007). In our solar system, Uranus and Neptune may scatter planetesimals into the Oort cloud more efficiently, largely due to their lower masses. However, they are not massive enough to scatter a Jupiter-mass planet into an Oort cloudlike orbit. Assuming that the planet formation typically produces a few giant planets per star, a typical cluster might form a few systems where a giant planet is scattered outward and be perturbed onto an Oort cloudlike orbit that will persist for billions of years. Although giant planets remaining in very long period orbits for billions of years will be rare, the number of giant planets at large separation may be greatly increased around young stars, since giant planets that have been scattered outward will typically spend less than 1 Myr on wide, eccentric orbits before becoming unbound. The chance of detecting such planets is further enhanced since the direct detection of giant planets is most practical while they are still young and radiating the heat of accretion in the infrared. Therefore, we explore the possibility of detecting giant planets that have recently been scattered outward, before they eventually become unbound.

3.1. Methods

3.1.1. Initial Conditions

We investigate whether planet scattering may produce a population of detectable planets on wide orbits by performing *N*-body integrations of "dynamically active" (= will undergo instability) planetary systems that typically contain three giant planets and three less massive planets. In the test particle limit of the less massive planets, systems with three giant planets represent simple systems that can undergo a dynamical instability after an extended period of seemingly regular orbital evolution (Marzari & Weidenschilling 2002; Chatterjee et al. 2008). This is in contrast to systems containing only two planets, which have a sharp

boundary dividing probably stable configurations from systems that rapidly result in close encounters (Gladman 1993). Three-planet systems have the additional advantage that they are more likely to retain signatures of possible prior instabilities (Veras & Armitage 2006). Although planetary systems may form even more planets, chaotic orbital evolution typically results in planets being ejected, accreting onto the star, or colliding with each other until only two or three planets remain (Papaloizou & Terquem 2001; Adams & Laughlin 2003). Due to the strongly chaotic evolution of dynamically active multiple-planet systems, systems with three or more giant planets behave qualitatively similar (Juric & Tremaine 2008).

We consider a realistic ensemble of postformation initial stellar masses, planet masses, and orbital separations. We draw stellar masses from two different initial mass functions (IMFs) and show that the results are broadly similar. We first utilize a simplistic IMF with a power-law exponent of -1.35 with mass cutoffs at 0.3 $M_{\odot}$ and 3.0 $M_{\odot}$, approximating the distribution of A through mid-M stars. We then apply rejection sampling in order to obtain a more realistic Miller–Scalo (Miller & Scalo 1979) power-law distribution (with exponents of -0.25, -1.0, and -1.3 for the mass ranges 0.3–1.0 $M_{\odot}$, 1.0–2.0 $M_{\odot}$, and 2.0–3.0 $M_{\odot}$, respectively). We report all data and figures from the Miller–Scalo power-law distribution, and where comparison is appropriate, data for the simple power-law IMF in square brackets. The comparisons will show that the results are insensitive to this choice of IMF at the $\sim$ 1% level.

We randomly draw six planet masses from a distribution uniform in the log of the planet–star mass ratio as suggested by radial velocity surveys (Cumming et al. 2008). The upper limit (10^{-2}) is based on the paucity of more massive planets around solar-type stars. The lower limit (9×10^{-6}) is near a terrestrial mass and is well beyond the reach of current direct imaging campaigns.

Theoretically, the site of giant planet formation is believed to occur predominantly beyond the location of the snow line. Therefore, we sample the innermost planet's semimajor axis uniformly from 3 to 7 AU according to a uniform-random distribution. The lower bound roughly corresponds to the location of the snow line in the minimum mass solar nebula (Lecar et al. 2006). Various environments can yield snow line locations which vary over 1 order of magnitude (Garaud & Lin 2007; Kennedy & Kenyon 2008). Therefore, our range of semimajor axes for the innermost planet allows for a variety of likely snow line locations.

We choose an initial spacing between neighboring planets constant in units of the mutual hill radius, K. Our choice of $K = 4.2$ almost guarantees that each system will undergo dynamical instability, and does so within a few million inner orbital times (see Figure 29 of Chatterjee et al. 2008). Thus, instabilities occur only after enough orbits that chaos has erased memory of the exact initial conditions. The value of K then effectively sets the timescale for instability in systems where we expect close encounters, collisions, and ejections to occur. Hence, our results should be interpreted in terms of the rate of detectable planets per *dynamically active* planetary system, rather than the rate relative to all stars or all planetary systems. Although our choice for the value of K sets the timescale for the initial onset of instability in our simulations, the final outcomes and the timescale for planets on wide, eccentric orbits to become unbound is not sensitive to K, but rather the mass of the interior planet that eventually ejects the planet (Pan & Sari 2004).

We randomly choose the orbital orientation and mean anomalies from uniform distributions, and assign the initial eccentricities and inclinations also from uniform distributions, bounded by < 0.01 and $< 0.01^{\circ}$. Because we begin each system with three relatively closely spaced massive planets, the systems will typically self-excite larger eccentricities and inclinations. In this paper, we focus our attention on planets that have undergone repeated close encounters with one or more planets before being scattered to very large ($\gtrsim$ 100 AU) separations. Thus, our conclusions will not be sensitive to the exact choice of initial semimajor axes, eccentricities, and inclinations.

3.1.2. Integration Methods

We integrate 1899 [2000] sets of initial conditions described above for 500 million years. We perform all integrations with the Burlirsch–Stoer integrator from the *Mercury N*-body integration package (Chambers 1999). In order to monitor the effects of ejected planets, planets were removed from the system only upon reaching a semimajor axis of 10^6 AU from their parent star. All integrations included the effects of possible collisions of planets with one another and with the parent star, but did not include fragmentation. A different set of 2000 integrations also included tidal effects from the galactic disk added to the function *mfo_user*, according to the prescription given by Higuchi et al. (2007):

$$\frac{d^2\vec{r}}{dt^2} = -GM_{\odot}\frac{\vec{r}}{r^3} - \nu_0^2\vec{z}, \tag{12}$$

where $\nu_0 = \sqrt{4\pi G\rho}$ is the vertical frequency and ρ is the density in the solar neighborhood. We assumed that $\rho = 0.1\ M_{\odot}\ \mathrm{pc}^{-3}$ (Holmberg & Flynn 2000). In addition to the disk tide, there is a radial component of the galactic tide due to the galactic bulge and dependent on the Sun's angular speed around the galactic center. Since the radial galactic tide operates on a timescale an order of magnitude longer than the disk tide Higuchi et al. (2007), we neglect this term.

In Section 4, we will discuss the prospects for observing such planets. In this section, we focus on the dynamical properties of these integrations.

3.2. Results

The numerical simulations described in Section 3 result in several qualitative outcomes. In each case, at least one of the six planets is ejected, collides with its parent star, or collides with one another. Any of these outcomes causes the planet to be removed from the simulation. The following lists the percent of systems with a given number of bound planets remaining at the end of the simulations (at 500 Myr), with the values in parentheses indicating the simulations which included the galactic tide: zero planet, 1.4% [1.2% (1.2%)]; one planet, 15.4% [15.6% (15.5%)]; two planets, 41.0% [41.3% (41.4%)]; three planets, 27.9% [27.9% (27.7%)]; four planets, 13.3% [13.0% (12.2%)]; five planets, 1.16% [1.15% (1.95%)]; six planets, 0% [0% (0%)]. Hence, the overall dynamical effect of the galactic tide on these simulations, after 500 Myr and over distances of 10^6 AU, is negligible. Further, two-planet systems are the most likely outcome of our planet–planet scattering simulations, with three-planet systems being the secondmost likely outcome; these results agree well with Figure 6 of Adams & Laughlin (2003), who use 10 planets and a similar initial mass distribution.

Although our simulations were run for 500 Myr, the vast majority of close encounters, collisions, and ejections occur well

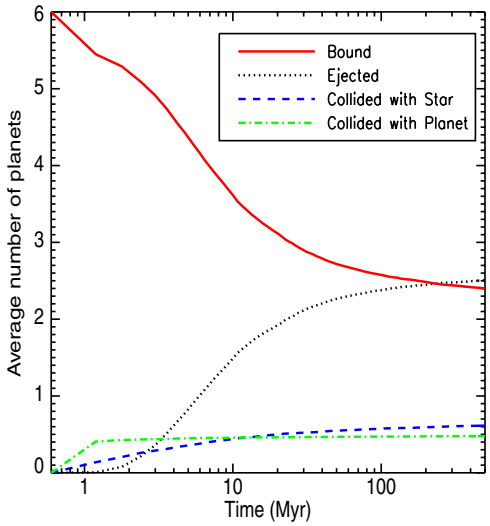

Figure 1. Average number of planets vs. time that remain bound to their star (red/solid line), get ejected (black/dotted), collide with the star (blue/dashed), and collide with another planet (green/dot-dashed).

(A color version of this figure is available in the online journal.)

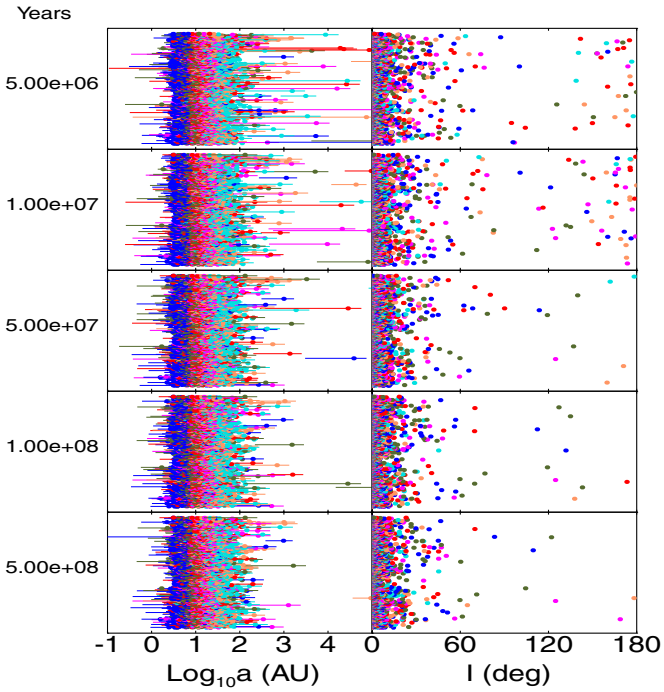

Figure 2. Snapshots showing the orbital properties of the surviving planets (of each system) with masses greater than 5×10^{-4} $M_{\odot}$ at five times from 5 (top) to 500 Myr (bottom). Within a panel, each row represents a different system. In the left panels, points indicate semimajor axes, and the horizontal lines indicate the pericenter and apocenter distances for each planet. In the right panels, points display inclination. The planet symbol colors indicate initial proximity to the star, and are given by blue/circles (innermost), green/crosses, red/squares, magenta/triangles, salmon/diamonds, and aqua/dots (outermost).

(A color version of this figure is available in the online journal.)

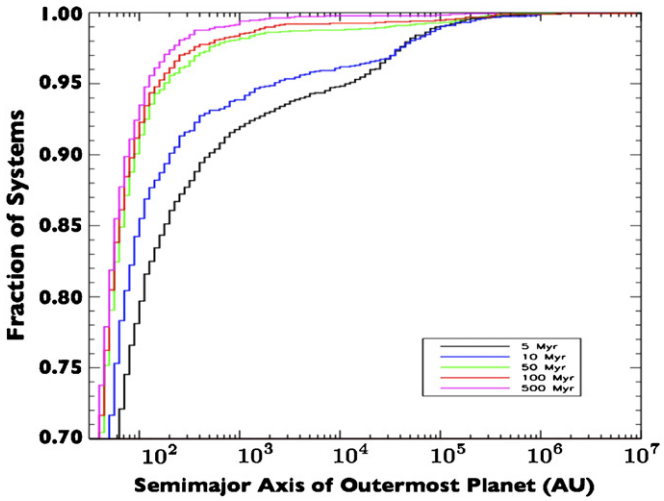

Figure 3. Cumulative histograms of the semimajor axis of the outermost bound planet at 5 Myr (black/solid lines), 10 Myr (blue/dotted lines), 50 Myr (green/dashed lines), 100 Myr (red/dot-dashed lines), and 500 Myr (magenta/triple-dot-dashed lines).

(A color version of this figure is available in the online journal.)

before 100 Myr. The *median* time to the first close encounter between any two planets or planet is $t \approx 9.04 \times 10^3$ [9.15×10^3] yr, and the *mean* time to the first close encounter was $t \approx 1.33 \times 10^6$ [1.30×10^6] yr. We take one Hill radii to be the maximum distance from a body which constitutes a close encounter. In order to help quantify the dynamical settling time of the systems, we plot the average number of planets remaining, planets ejected, and planets suffering a collision as a function of time in Figure 1. The figure demonstrates that approximately half of the planets in each system still remain after 2×10^7 yr, and that ejections (as opposed to collisions) become the predominant removal mechanism after 30 Myr. After 2×10^8 yr, on average, more planets have been ejected than remain. Further, the fraction of planet–planet collisions are approximately equal to the fraction of planet–star collisions, but the latter dominates after 1×10^7 yr. At the end of our simulations, on average we can expect a system to still have between two and three planets. On even longer timescales we suspect that just a few more planets might be removed from the systems.

Figure 2 presents snapshots of the semimajor axes, periastron distances, and apoastron distances for each of the bound planets remaining with masses greater than 5×10^{-4} $M_{\odot}$ (a representative observational constraint) at times of 5, 10, 50, 100, and 500 Myr. Each row represents a different system, and the five panels, in descending order, contain 3583, 3476, 3227, 3164, and 3056 [3737, 3623, 3364, 3298, and 3186] planets (from an initial population of 12,000 planets). For the simple power law, without the mass constraint, the total number of bound planets at each of those five times would be [7537, 6805, 5403, 5122, and 4783]. The horizontal lines indicate the periastron–apoastron range of each planet, and the points indicate the semimajor axes. Color indicates the initial ordering in terms of semimajor axis, as described in the caption. Because planets that have been scattered beyond 100 AU are typically the least massive planets in the system, and there does not appear to be a significant correlation with the initial ordering (in terms of semimajor axes). By 5 and 10 Myr, the planet scattering has significantly excited planetary inclinations, but inclinations of $\approx 90^\circ \lesssim i \lesssim 150^\circ$ are rarer than those of $\approx 150^\circ \lesssim i \lesssim 180^\circ$. We find 0.5% [0.5%] of all planets at 5 Myr both harbor semimajor axes above 100 AU and are on retrograde orbits, but these planets are typically ejected after several 10^7 yr.

The planets of greatest interest to observational searches are those on "wide" orbits, with semimajor axes of tens, hundreds or thousands of astronomical units. The number of planets surviving beyond 1000 AU declines rapidly from 10 Myr to

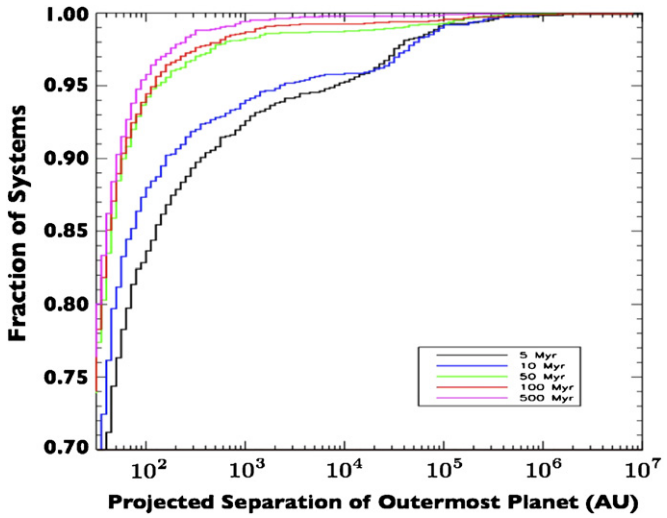

Figure 4. Cumulative histograms of the projected separation of the outermost bound planet at 5 Myr (black/solid lines), 10 Myr (blue/dotted lines), 50 Myr (green/dashed lines), 100 Myr (red/dot-dashed lines), and 500 Myr (magenta/triple-dot-dashed lines).

(A color version of this figure is available in the online journal.)

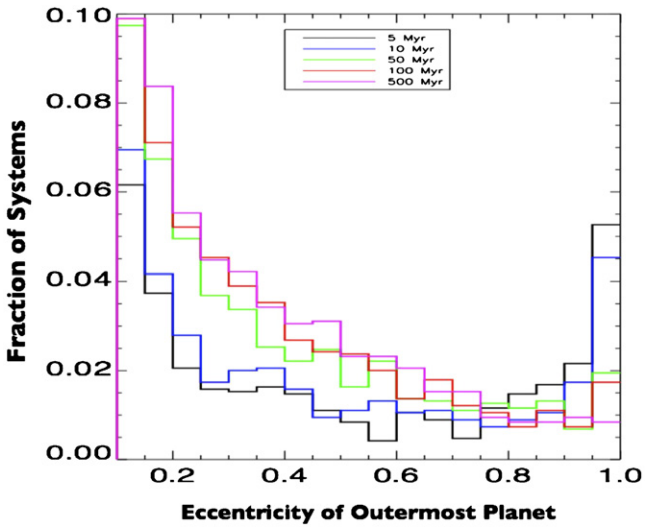

Figure 5. Histogram of the eccentricity of the outermost bound planet at 5 Myr (black/solid lines), 10 Myr (blue/dotted lines), 50 Myr (green/dashed lines), 100 Myr (red/dot-dashed lines), and 500 Myr (magenta/triple-dot-dashed lines). The bound planets with nearly parabolic orbits are prevalent for several tens of megayears, but eventually become unbound.

(A color version of this figure is available in the online journal.)

50 Myr, but even at 500 Myr, planets remain beyond 1000 AU. In Figure 3, we present a cumulative distribution for the semimajor axis of the outermost surviving planet from $10^{1.5}$to 10^7 AU at 5 Myr (black/solid lines), 10 Myr (blue/dotted lines), 50 Myr (green/dashed lines), 100 Myr (red/dot-dashed lines), and 500 Myr (magenta/triple-dot-dashed lines). The ejection of many planets (especially between 10 and 50 Myr) partially accounts for the difference between the two sets of curves (compare the 5 and 10 Myr curves to the 50, 100, and 500 Myr curves). Fewer planets reside beyond 40 AU at 5 Myr than at 10 Myr because many systems are still undergoing significant dynamical evolution at 10 Myr. Between 10 and 100 Myr, the number of planets on wide orbits decreases, since the rate of planets being scattered outward into wide orbits is less than the rate of planets already on wide orbits becoming unbound. At 100 Myr, less than 0.1% of systems harbor planets with semimajor axes beyond 10^5 AU. Although small, such planets could be present in a cluster of thousands of stars.

Unfortunately, determining the semimajor axes of planets on very wide orbits is difficult because the orbital timescale greatly exceeds the typical time span of observations. Instead, direct imaging measures the star–planet separation projected onto the plane of the sky. In order to evaluate the detectability of such planets, we present cumulative distributions for the projected separation in Figure 4. In order to improve our statistics, we calculate the projected separation for each of five times and 10 viewing geometries (by drawing the mean anomaly, pericenter angle, and $\cos(i)$ from uniform random distributions). For nearly circular orbits, the planet–star separation remains close to the semimajor axis throughout the orbit, and the projected separation averages to be $\simeq$ 0.7 times the semimajor axis. For highly eccentric orbits, the planet spends most of its time near apocenter, so that the average projected separation can exceed the semimajor axis, depending on the orientation of the orbit relative to the line of sight. We find that the two effects approximately cancel for planets on wide orbits. The cumulative distributions in Figures 3 and 4 differ by just a few percent.

Next, we investigate the eccentricities of the planets that have been scattered onto wide orbits. Previous studies have compared the eccentricities of planets after planet scattering to radial velocity observations. For example, two-planet scattering rarely results in an inner planet eccentricity greater than 0.8 following the ejection of another planet (Ford & Rasio 2008). Similarly, three-planet scattering results in only a modest fraction of inner planets with eccentricities greater than 0.8 (Chatterjee et al. 2008). In this study, we focus instead on the eccentricities of planets that have been scattered outward. Although many of these planets will eventually become unbound, we consider the eccentricity distribution of all planets still bound at each of several ages in Figure 5. The black/solid, blue/dotted, green/dashed, red/dot-dashed, and magenta/triple-dot-dashed lines on this histogram correspond to 5, 10, 50, 100, and 500 Myr. The last bin demonstrates that the number of planets on nearly parabolic ($e > 0.95$) orbits decreases with time, where the greatest difference is between the 10 and 50 Myr curves. Taken together, Figures 3 and 5 indicate that planets on the verge of ejection typically have nearly linear orbits, spending the vast majority of the time near apocenter, but receiving a "kick" once each orbit when they briefly sweep into the inner portion of the planetary system (Pan & Sari 2004). In our simulations, less massive planets are preferentially scattered into wide orbits. The majority of these planets are less than a Jupiter mass, but only a few percent exceed 4 $M_{\rm Jup}$.

Figures 3–5 do not include planets that have already been ejected onto hyperbolic orbits ($e > 1$). An unbound planet will quickly become undetectable to a coronagraphic direct imaging search with a relatively small field of view (FOV). Assuming a planet with an ejection velocity of $\sim GM_\star/a$, the ejected planet would have traveled more than 10^5 AU away from the host star (beyond a_t) in $\sim 10^5$ yr. As a result, directly detecting an ejected planet still in the vicinity of its parent star is improbable. However, such planets may still be detectable as free-floating planets by imaging of more distant star-forming regions with a large FOV.

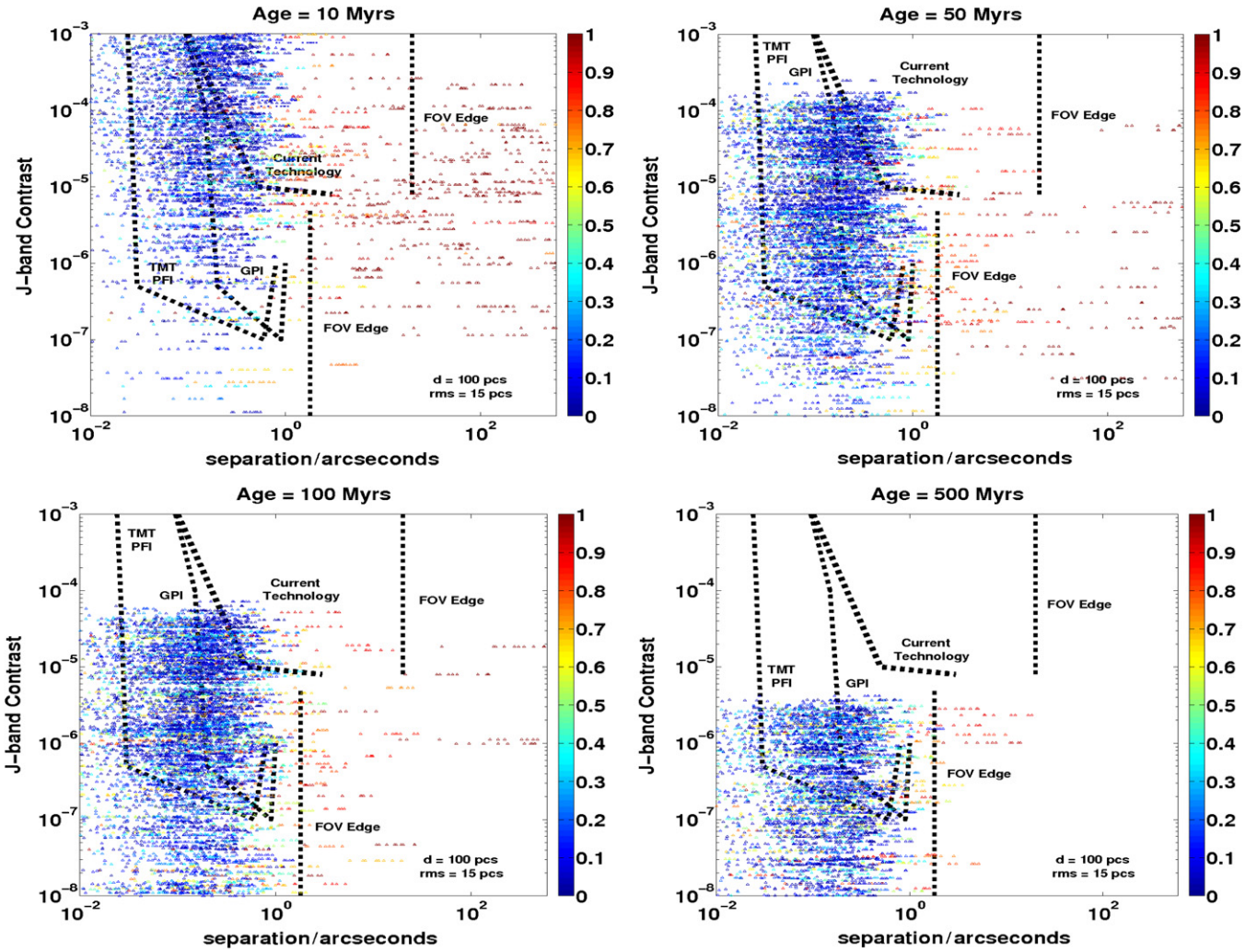

Figure 6. Contrast vs. angular separation for a population of exoplanets as a function of age. The data points are color-coded/grayscaled according to eccentricity. The circles indicate that all six planets in a given system remained gravitationally bound. The triangles indicate that at least one of the planets became unbound. The dashed lines indicate the approximate range of detectability based on current and ground-based direct imaging searches. The companions located exterior to the FOV edge are not detectable. The estimates for the GPI and the TMT PFI are somewhat conservative, as they could achieve deeper effective contrasts by a factor of order unity.

(A color version of this figure is available in the online journal.)

4. DETECTABILITY OF LONG-PERIOD PLANETS

Here, we investigate the plausibility of detecting planets at large separations with direct detection campaigns. We take snapshots of each planetary system from the previous section at several times: 5, 10, 50, 100, and 500 Myr, all times for which Baraffe et al. (2008) provide theoretical models. The first two snapshots are particularly relevant for direct imaging of very young stars, typically of star-forming regions $\sim$ 100 pc from the Sun. In those locations, models predict that giants planets will be significantly more luminous in the *J* band than a blackbody of the same temperature. The 100 and 500 million year snapshots are particularly relevant for observations of nearby stars. At these later ages, models predict that planets have cooled enough that the *J*-band luminosity is dramatically reduced, so the *L*-band observations may become more favorable.

For direct imaging to detect planetary systems like our solar system, it is important to focus on the closest young stars (at $\approx$ 100 pc), where the inner working angle corresponds to a small physical separation. Most young stars in the immediate solar neighborhood are believed to have formed in small groups or associations, in which case the processes described in Section 2.2 will not be relevant. However, these same direct imaging campaigns may overlook young giant planets on wide orbits, as they lie beyond the coronagraph's outer working angle. When searching for planets at wide separations, it is possible or even advantageous to target more distant star-forming regions. Thus, it would be possible to search for planets that formed in more substantial clusters at a variety of ages.

4.1. Detection Criteria

Snapshots of each planetary system from the previous section at 10, 50, 100, and 500 Myr are plotted in terms of contrast and angular separation in Figure 6. Contrast is calculated by comparing the absolute magnitude of the planet to that of its host. We use the atmospheric models of Girardi et al. (2002) and Baraffe et al. (2003) (and I. Baraffe et al. 2008, private communication) to find the brightness of the stars and exoplanets, respectively. In Figure 6, we assume that a cluster of stars, each with metalicity $Z = 0.019$, is located at an average distance of 100 pcs from the Sun with an rms scatter of 15 pcs. In Figure 7, we place the same stars at 60 pcs with an rms scatter of 20 pcs. In each case, their positions within these limits

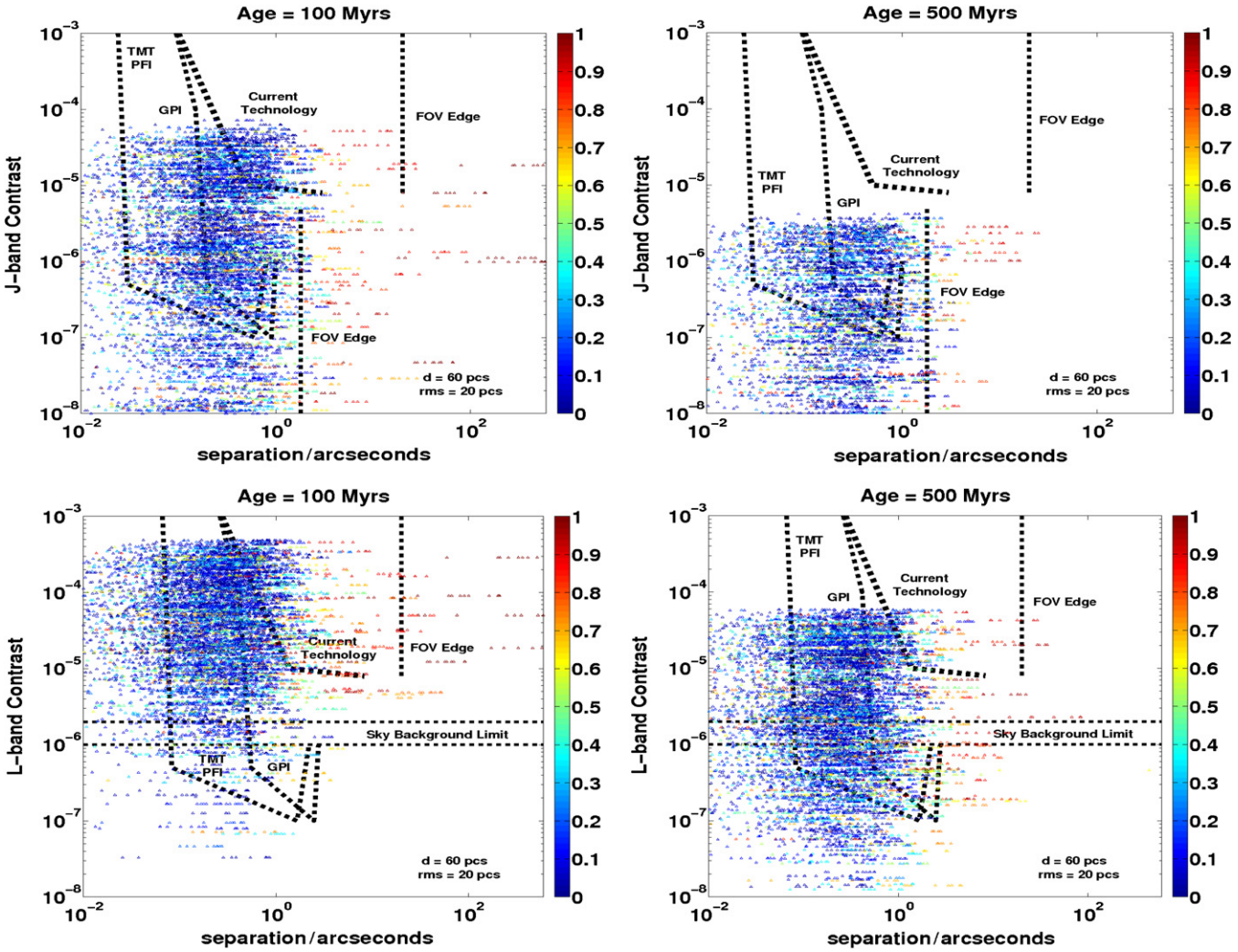

Figure 7. Contrast vs. angular separation for a nearby population of exoplanets in the *J* (upper panels) and *L* (lower panels) bands. Planets are brighter in the *L* band at older ages, but the sky background is at least 10^{-6} times as bright as the brightest stars *after* subtraction and places a hard limit on ground-based sensitivities. The GPI is unlikely to conduct observations in the *L* band.

(A color version of this figure is available in the online journal.)

are randomized. For reference, we also include approximate detection sensitivities from recent AO-coronagraph surveys (namely, Biller et al. 2007; Kasper et al. 2007; Lafrenière et al. 2007; Nielsen et al. 2007) as well as future instruments, such as GPI (Macintosh et al. 2006a) and the proposed Thirty Meter Telescope Planet Formation Imager (TMT PFI; Macintosh et al. 2006b).

Models predict that giant planets will be several orders of magnitude more luminous in the near-IR bands compared with a blackbody of the same temperature at such young ages. The first two snapshots (10 and 50 Myr, the top two panels of Figure 6) are particularly relevant for searching members of star-forming regions. At these two times we selected the *J* band ($\bar{\lambda} = 1.25$ μm) because it offers the brightest planets, best spatial resolution, and faintest sky background in a regime where the atmosphere can still be adequately controlled with AO.

The 100 and 500 Myr snapshots are more relevant for observations of nearby moving groups, such as Hyades or the Ursa Majoris cluster. At these late stages, models predict that planets have cooled enough that the *J*-band luminosity is dramatically reduced. In this case, the *L*-band observations, $\bar{\lambda} = 3.8$ μm, may become favorable for large angular separations (Heinze 2007). There is, however, a tradeoff, because the *L* band has the disadvantage of a bright and rapidly fluctuating sky background (Phillips et al. 1999), which ultimately limits sensitivity (Figure 7). Chopping and nodding techniques can only subtract out this source of noise (plus instrument and detector noise) to one part in $\approx 10^5$, even when operating at the photon noise limit. In the best case scenario, this translates to contrast levels of $\approx 10^{-6}$, i.e., when targeting stars with apparent magnitudes $L < 4$. The prospects are better by nearly an order of magnitude when conducting observations at the South Pole, but constructing single-dish telescopes with sufficient angular resolution is currently difficult given the harsh conditions.

It is also worth noting that the sensitivity of specialized high-contrast imaging instruments is nonmonotonic with angular separation. This is due to the explicit removal of instrument scattered light within the controllable spatial frequencies of the AO system deformable mirror. The number of actuators and their spacing defines this primary search area—the so-called dark-hole (Trauger & Traub 2007). GPI's FOV is 3.″6. Current high-resolution instruments have somewhat larger FOVs (e.g., Hayward et al. 2001).

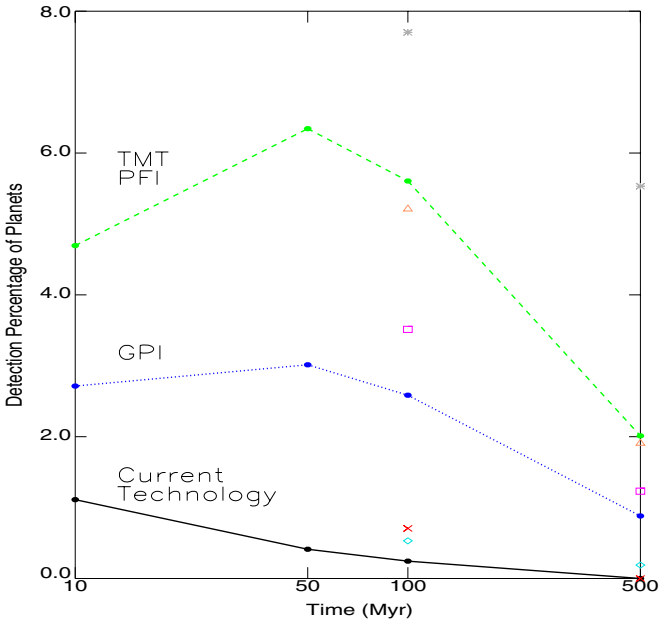

Figure 8. Percent of all planets from an enhanced distribution (where 10 viewing geometries for each initially six-planet system are included) which are detectable within the bounds imposed in Figures 6 and 7 according to current technology (solid/black curve), GPI (blue/dotted curve), and TMT PFI (green/dashed curve) in the J band for a cluster located at an average distance of 100 pcs from the Sun with an rms scatter of 15 pcs. All isolated symbols refer to a cluster located at an average distance of 60 pcs from the Sun with a RMS scatter of 20 pcs and represent the fraction of planets which are: currently detectable by J-band (red crosses); GPI detectable by J-band (magenta squares); TMT PFI detectable by J-band (salmon triangles); currently detectable by L-band (aqua diamonds); and TMT PFI detectable by L-band (grey asterisks).

(A color version of this figure is available in the online journal.)

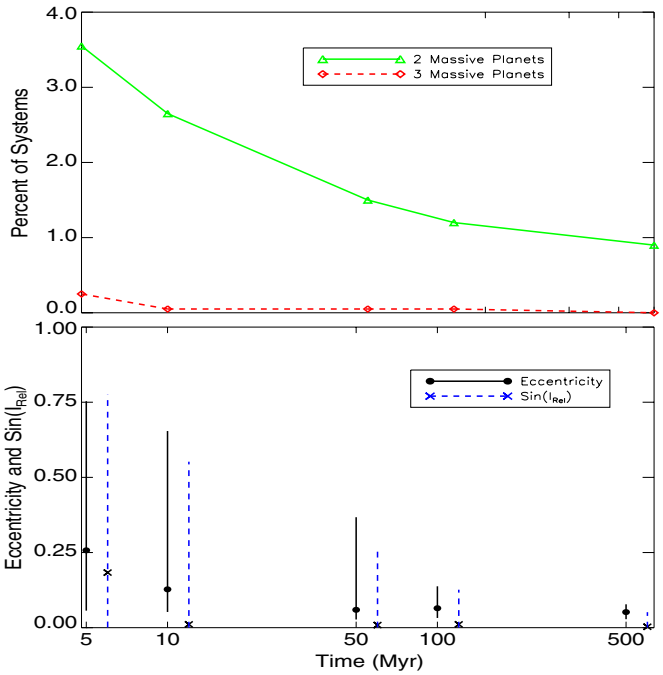

Figure 9. Statistics of systems with multiple bound planets all on wide orbits (projected separation $\geqslant$ 40 AU) as a function of age. The upper panel plots the fraction of all systems with two (green/solid line and triangles) and three (red/dashed line and diamonds) massive ($\geqslant 0.3 M_J$) planets remaining beyond 40 AU. The lower panel showcases the median eccentricities (dots and black/solid lines) and sine of the relative inclinations (crosses and blue/dashed lines) of all systems with two planets on wide orbits, and their 25–75 percentile ranges. The blue/dashed lines are slightly offset from the other lines for clarity.

(A color version of this figure is available in the online journal.)

Finally, in Figure 8, we plot the fraction of orbit realizations of all planets which would be detectable according to Figures 6 and 7 as a function of age, band, and separation. We emphasize that this fraction is representative of all planets in dynamically active systems (those which undergo instability), according to our initial conditions. Current technology should allow for the direct imaging detection of planets at ages $\lesssim$ 100 Myr, whereas GPI and TMT PFI are predicted to discover several times more planets. Both instruments are likely to discover the greatest number of planets at an age of $\approx$ 50 Myr. Importantly, current J-band (red crosses) and L-band (aqua diamonds) observations demonstrate the slight improvement the latter affords at later times; the projected TMT PFI observations in the J band (salmon triangles) and the L band (gray asterisks) demonstrate the marked improvement the L band provides at both 100 and 500 Myr.

5. DISCUSSION

We have shown that planets could survive in very wide orbits. For the relatively young stars typically surveyed by direct imaging campaigns, planets could survive at distances of up to the tidal limit. As for a potential formation mechanism, we consider the role of planet–planet scattering, with a focus on the implications for long-period planets. Because the process of planet–planet scattering typically extends for tens of millions of years, most stars will not remain in a high-density stellar environment long enough for close stellar encounters to be effective at removing long-period planets (with $a < a_t, a_{\rm ps}$; see Equations (1) and (3)).

We performed direct N-body simulations of dynamically active planetary systems, including the effects of galactic tides, and show that the planet scattering can indeed form long-period planets. Of particular interest, we found that at ages of $\simeq$ 10–50 Myr, there is a sizable population of planets on wide and highly eccentric orbits. Although most of these planets will eventually be ejected, they can persist on wide orbits for several tens of millions of years. We caution that our models predict a significant temporal evolution of this population. Therefore, statistical analyses of direct imaging surveys should account for the possibility of a time-variable population of planets on wide orbits.

We considered the detectability of the planets scattered into long-period orbits in our simulations. Planet models are highly uncertain, largely due to the uncertainty in initial conditions (e.g., Martin et al. 2007). Nevertheless, we show that even assuming "cold-start" models, direct imaging surveys are already sensitive to giant planets in nearby star-forming regions. Future direct imaging surveys will become sensitive to both closer planets and planets with smaller luminosities.

Recent interest in the candidate three-planet HR 8799 system (Marois et al. 2008) motivates us to consider the multiplicity of planets from the same system all in bound wide orbits. The properties (such as eccentricity and inclination) of the orbits of those three planets are largely unconstrained at the present time. The planet masses are approximated to lie in the 5–13 $M_{\rm Jup}$ range and the projected separations are estimated to be 24, 38, and 68 AU (Marois et al. 2008). In our simulations of Section 3, the initial semimajor axis of the outermost planet is typically 15–30 AU, so any planets beyond 40 AU have undergone

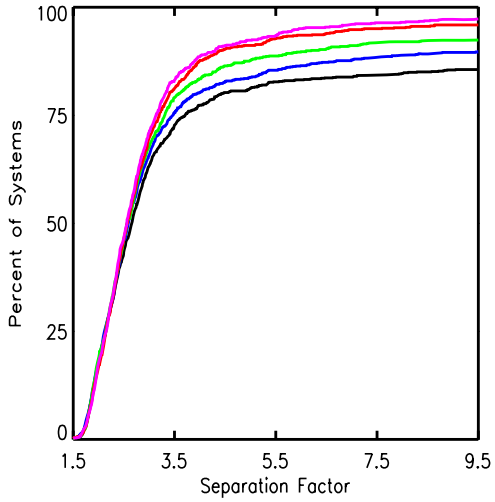

Figure 10. Mutual separations of outermost three planets in each system, such that each adjacent pair of the outermost three planets has a projected separation within a factor of the values on the *X*-axis. The black/solid, blue/dotted, green/dashed, red/dot-dashed, and magenta/dot-dot-dot-dashed lines refer to snapshots at 30, 40, 50, 100, and 150 Myr.

(A color version of this figure is available in the online journal.)

significant scattering. In order to evaluate the frequency of multiple planets at wide separations due to planet scattering, we tally how many systems contain multiple planets on bound orbits with semimajor axes exceeding 40 AU and masses exceeding 5×10^{-4} $M_{\odot}$. At (5, 10, 50, 100, 500) Myr, (71, 53, 30, 24, 18) [76, 59, 34, 26, 19] systems contain two such planets and (5, 1, 1, 1, 0) [7, 1, 1, 1, 0] systems contain three or more such planets (see Figure 9).

These results suggest that 3.8% (0.9%) of dynamically active planetary systems could contain multiple massive planets on wide orbits at ages of 5 Myr (500 Myr and beyond). Further, 66% (40%) of systems containing multiple planets on wide orbits with ages less than 10 Myr (100 Myr) will become unstable on longer timescales. This model predicts that multiple planets on wide orbits will become less common with increasing stellar age (Figure 9). Figure 10 also demonstrates this trend by displaying the percent of systems with each adjacent pair of the outermost three planets having a projected separation within factors appearing on the *X*-axis. The black, blue, green, red, and magenta curves refer to data at 30, 40, 50, 100, and 150 Myr, ages chosen to correspond to the likely age of the three planets in HR 8799 (Marois et al. 2008). On this plot, $<$ 1% of all our systems simulated would be as "packed" as HR 8799 (with an X value of $38/24 = 1.58$), suggesting that the planets in that system are unlikely to have been scattered to those locations without resonant locking (Fabrycky & Murray-Clay 2008) or migrating through a disk.

Young systems containing multiple planets at wide separations would be expected to have sizable eccentricities, even larger than the extrasolar planet average. With time, two-planet systems with large eccentricities tend to be destroyed, so the average eccentricity decreases to a more modest value (0.14), very similar to that observed for multiple-planet systems discovered by radial velocity searches (Wright et al. 2009). The average relative inclination between two planets on wide orbits also decreases with time from 28.4% to 9.5% degrees between 10 and 500 Myr. These results can be used to inform the interpretation and dynamical modeling of multiple-planet systems found by direct imaging (Fabrycky & Murray-Clay 2008).

In the future, comparing the frequency of long-period planets as a function of stellar age could provide a significant constraint on planet formation models. Such observations could determine the timescale for the onset of strong instabilities in multiple-planet systems and place constraints on the typical number of giant planets formed (which may be greater than the number of giant planets around mature stars). Such constraints would be particularly interesting, when combined with constraints on free-floating planets from direct imaging of star-forming regions and/or gravitational microlensing observations.

In our simulations excluding the galactic tide, 40% [42%] of all planets (totaling 13.6% [13.7%] of the planetary mass) were ejected. Of the planets ejected, 21.2% (28.9%) [21.0% (28.9%)] had a mass (mass ratio) greater than 0.3 $M_{\rm Jup}$ (0.3 $M_{\rm Jup}/M_{\odot}$) and 54.1% (60.1%) [54.2% (60.1%)] of planets had a mass (mass ratio) between $5M_{\oplus}$ ($5M_{\oplus}/M_{\odot}$) and 0.3 $M_{\rm Jup}$ (0.3 $M_{\rm Jup}/M_{\odot}$). The simulations which included the effects from the galactic tide yielded nearly identical results, varying the above values by at most by a few percent. All these ejected planets would become free-floating planets. After they fade and become undetectable by direct imaging, the best chance for detecting this population of planets is via gravitational microlensing. Although the optical depth for microlensing is independent of the mass function of free-floating planets, the event rate and event timescale are sensitive to the mass function. The event rate for ejected microlensing planets which are more massive than 0.3 $M_{\rm Jup}$ (0.3 $M_{\rm Jup}/M_{\odot}$) is 56.6% (64.4%) [56.2% (64.4%)] of the total event rate for all unbound masses, but other mass bins will produce different event rates. In order to better quantify this depends on the mass, we bin the masses uniformly in log M and for sufficiently high sampling, estimate that a power-law index of [$\approx$ 0.37] approximates the positive correlation between event rate (as the dependent variable) and mass.

In reality, there would be additional microlensing events due to (1) planets still bound to their parent stars and (2) small planets or protoplanets that were not included in our simulations. Therefore, the above numbers should be interpreted as a lower limit. Regarding the contribution from bound planets, 38.0% [39.9%] of all the initial planets (totaling 81.5% [81.3%] of the planetary mass) remain bound. Of these, 76.5% (84.1%) [76.2% (84.1%)] had a mass (mass ratio) greater than 0.3 $M_{\rm Jup}$ (0.3 $M_{\rm Jup}/M_{\odot}$), and accounted for 93.8% (96.4%) [93.6% (96.4%)] of the overall microlensing event rate. Unfortunately, existing surveys are prone to missing short-duration events and hence biased toward finding more massive planets (especially for free-floating planets where there is not a longer duration stellar microlensing event to trigger intensive observations). These results suggest that a microlensing survey that efficiently detected the short events due to free-floating terrestrial planets would provide a useful diagnostic for the rate at which terrestrial planets form in dynamically active systems (relative to the rate of giant planet formation in similar systems). When combined with statistical information about the frequency of terrestrial and giant planets in mature planetary systems, this synergy would provide a probe of the chaotic phase of planet formation and a test of the planet–planet scattering model for exciting eccentricities of extrasolar planets.

We considered the detectability of the planets scattered into long-period orbits in our simulations. Indeed, planet models are highly uncertain, largely due to the uncertainty in initial conditions (e.g., Martin et al. 2007). We show that even assuming "cold-start" models, direct imaging surveys are already sensitive to giant planets in nearby star-forming regions. Future direct

imaging surveys will become sensitive to both closer planets and planets with smaller luminosities.

We thank the anonymous referee for his keen observations, and Daniel Apai, John Chambers, Vacheslav Emel'yanenko, Daniel Fabrycky, Elizabeth Lada, Eduardo Martin, Michael Meyer, Ruth Murray-Clay, Steinn Sigurdsson, Jonathan Tan, and Scott Tremaine for sharing their insights. The authors acknowledge the University of Florida High-Performance Computing Center for providing computational resources and support that have contributed to the research results reported within this paper.

REFERENCES

Adams, F. C., & Laughlin, G. 2003, Icarus, 163, 290
Adams, F. C., Proszkow, E. M., Fatuzzo, M., & Myers, P. C. 2006, ApJ, 641, 504
Armitage, P. J. 2007, arXiv:astro-ph/0701485
Baraffe, I., Chabrier, G., & Barman, T. 2008, A&A, 482, 315
Baraffe, I., Chabrier, G., Barman, T. S., Allard, F., & Hauschildt, P. H. 2003, A&A, 402, 701
Biller, B. A., et al. 2007, ApJS, 173, 143
Bonatto, C., & Bica, E. 2009, arXiv:0901.0833
Boss, A. P. 2006, ApJ, 637, L137
Brasser, R., Duncan, M. J., & Levison, H. F. 2007, Icarus, 191, 413
Cai, K., Durisen, R. H., Michael, S., Boley, A. C., Mejía, A. C., Pickett, M. K., & D'Alessio, P. 2005, in Proc. Conf., Protostars and Planets V, ed. B. Reipurth, D. Jewitt, & K. Keil (Tuscon, AZ: Univ. of Arizona Press), 8155
Chambers, J. E. 1999, MNRAS, 304, 793
Chambers, J. E. 2006, ApJ, 652, L133
Chatterjee, S., Ford, E. B., Matsumura, S., & Rasio, F. A. 2008, ApJ, 686, 580
Cumming, A., Butler, R. P., Marcy, G. W., Vogt, S. S., Wright, J. T., & Fischer, D. A. 2008, PASP, 120, 531
Debes, J. H., & Sigurdsson, S. 2006, A&A, 451, 351
de la Fuente Marcos, C., & de la Fuente Marcos, R. 2001, A&A, 371, 1097
de la Fuente Marcos, R., & de la Fuente Marcos, C. 2008, ApJ, 672, 342
Dodson-Robinson, S. E., Bodenheimer, P., Laughlin, G., Willacy, K., Turner, N. J., & Beichman, C. A. 2008, ApJ, 688, L99
Dones, L., Weissman, P. R., Levison, H. F., & Duncan, M. J. 2004, in Comets II, ed. M. C. Festou, H. U. Keller, & H. A. Weaver (Tucson, AZ: University of Arizona Press) 153
Duncan, M., Quinn, T., & Tremaine, S. 1987, AJ, 94, 1330
Durisen, R. H., Boss, A. P., Mayer, L., Nelson, A. F., Quinn, T., & Rice, W. K. M. 2007, in Proc. Conf., Protostars and Planets V, ed. B. Reipurth, D. Jewitt, & K. Keil (Tuscon, AZ: Univ. of Arizona Press), 607
Fabrycky, D. C., & Murray-Clay, R. A. 2008, arXiv:0812.0011
Ford, E. B., & Chiang, E. I. 2007, ApJ, 661, 602
Ford, E. B., Havlickova, M., & Rasio, F. A. 2001, Icarus, 150, 303
Ford, E. B., Joshi, K. J., Rasio, F. A., & Zbarsky, B. 2000a, ApJ, 528, 336
Ford, E. B., Kozinsky, B., & Rasio, F. A. 2000b, ApJ, 535, 385
Ford, E. B., & Rasio, F. A. 2008, ApJ, 686, 621
Fregeau, J. M., Chatterjee, S., & Rasio, F. A. 2006, ApJ, 640, 1086
Garaud, P., & Lin, D. N. C. 2007, ApJ, 654, 606
Girardi, L., Bertelli, G., Bressan, A., Chiosi, C., Groenewegen, M. A. T., Marigo, P., Salasnich, B., & Weiss, A. 2002, A&A, 391, 195
Gladman, B. 1993, Icarus, 106, 247
Goldreich, P., et al. 2004, ARA&A, 42, 529
Gomes, R., Levison, H. F., Tsiganis, K., & Morbidelli, A. 2005, Nature, 435, 466
Haisch, K. E., Lada, E. A., Jr., & Lada, C. J. 2001, ApJ, 553, L153
Hayward, T. L., Brandl, B., Pirger, B., Blacken, C., Gull, G. E., Schoenwald, J., & Houck, J. R. 2001, PASP, 113, 105
Heinze, A. N. 2007, PhD thesis, Univ. of Arizona
Higuchi, A., Kokubo, E., Kinoshita, H., & Mukai, T. 2007, AJ, 134, 1693
Higuchi, A., Kokubo, E., & Mukai, T. 2006, AJ, 131, 1119
Holmberg, J., & Flynn, C. 2000, MNRAS, 313, 209
Hubickyj, O., Bodenheimer, P., & Lissauer, J. J. 2005, Icarus, 179, 415
Hut, P. 1983, ApJ, 268, 342
Juric, M, & Tremaine, S. 2008, ApJ, 686, 603
Kalas, P., et al. 2008, Science Express, 322, 1345
Kasper, M., Apai, D., Janson, M., & Brandner, W. 2007, A&A, 472, 321
Kennedy, G. M., & Kenyon, S. J. 2008, ApJ, 673, 502
Lafrenière, D., et al. 2007, ApJ, 670, 1367
Laughlin, G., & Adams, F. C. 1998, ApJ, 508, L171
Lecar, M., Podolak, M., Sasselov, D., & Chiang, E. 2006, ApJ, 640, 1115
Levison, H. F., Lissauer, J. J., & Duncan, M. J. 1998, AJ, 116, 1998
Macintosh, B., et al. 2006a, in SPIE Proc. 6272, Advances in Adaptive Optics II, ed. B. L. Ellerbroek & D. B. Calia (Bellingham, WA: SPIE), 62720L
Macintosh, B., et al. 2006b, in SPIE Proc. 6272, Advances in Adaptive Optics II, ed. B. L. Ellerbroek & D. B. Calia (Bellingham, WA: SPIE), 62720N
Marley, M. S., Fortney, J. J., Hubickyj, O., Bodenheimer, P., & Lissauer, J. J. 2007, ApJ, 655, 541
Marois, C., et al. 2008, Science Express, 322, 1348
Martin, R. G., Lubow, S. H., Pringle, J. E., & Wyatt, M. C. 2007, MNRAS, 378, 1589
Marzari, F., & Weidenschilling, S. J. 2002, Icarus, 156, 570
McCarthy, C., & Zuckerman, B. 2004, AJ, 127, 2871
Mejía, A. C., Durisen, R. H., Pickett, M. K., & Cai, K. 2005, ApJ, 619, 1098
Miller, G. E., & Scalo, J. M. 1979, ApJS, 41, 513
Moorhead, A. V., & Adams, F. C. 2005, Icarus, 178, 517
Morbidelli, A., Levison, H. F., Tsiganis, K., & Gomes, R. 2005, Nature, 435, 462
Nielsen, E. L., Close, L. M., Biller, B. A., Masciadri, E., & Lenzen, R. 2008, ApJ, 674, 466
Pan, M., & Sari, R. 2004, AJ, 128, 1418
Papaloizou, J. C. B., & Terquem, C. 2001, MNRAS, 325, 221
Phillips, A., Burton, M. G., Ashley, M. C. B., Storey, J. W. V., Lloyd, J. P., Harper, D. A., & Bally, J. 1999, ApJ, 527, 1009
Pollack, J. B., Hubickyj, O., Bodenheimer, P., Lissauer, J. J., Podolak, M., & Greenzweig, Y. 1996, Icarus, 124, 62
Rafikov, R. R. 2005, ApJ, 621, L69
Rafikov, R. R. 2007, ApJ, 662, 642
Rasio, F. A., & Ford, E. B. 1996, Science, 274, 954
Scharf, C., & Menou, K. 2009, ApJ, 693, L113
Stamatellos, D., & Whitworth, A. P. 2009, in AIP Conf. Proc. 1094, Cool Stars, Stellar Systems, and the Sun, ed. E. Stempels (Melville, NY: AIP), 557
Thomess, E. W., Duncan, M. J., & Levison, H. F. 1999, Nature, 402, 635
Thomess, E. W., Duncan, M. J., & Levison, H. F. 2002, AJ, 123, 2862
Throop, H. B., Bally, J., Esposito, L. W., & McCaughrean, M. J. 2001, Science 292, 1686
Trauger, J. T., & Traub, W. A. 2007, Nature, 446, 771
Tremaine, S. 1993, in in ASP Conf. Ser. 36, Planets Around Pulsars, ed. J. A. Phillips, S. E. Thorsett, & S. R. Kulkarni (San Francisco, CA: ASP), 335
Tsiganis, K., Gomes, R., Morbidelli, A., & Levison, H. F. 2005, Nature, 435, 459
Veras, D., & Armitage, P. J. 2004, MNRAS, 347, 613
Veras, D., & Armitage, P. J. 2006, ApJ, 645, 1509
Weidenschilling, S. J., & Marzari, F. 1996, Nature, 384, 619
Weinberg, M. D., Shapiro, S. L., & Wasserman, I. 1987, ApJ, 312, 367
Wright, J. T., Upadhyay, S., Marcy, G. W., Fischer, D. A., Ford, E. B., & Johnson, J. A. 2009, ApJ, 693, 1084